

Supramolecular assembly of optical solitons via long-range interactions

W. He¹, M. Pang^{1*}, J. Huang¹, C. R. Menyuk^{1,2}, P. St.J. Russell¹

Affiliations:

¹Max Planck Institute for the Science of Light, Staudtstrasse 2, 91058 Erlangen, Germany.

²Department of Computer Science and Electrical Engineering, University of Maryland Baltimore County, Baltimore, Maryland 21250, USA.

*Correspondence to: meng.pang@mpl.mpg.de

Abstract: Binding of particles through weak interactions plays a central role in multiple modern disciplines, from Cooper pairing of electrons in superconductivity to formation of supramolecules in biochemistry. Analogous in many ways to particles, optical solitons arising from a balance between nonlinearity and dispersion are extensively studied in many sub-fields of optics and photonics. Supramolecular assemblies of such particle-like light have, however, escaped experimental observations, and long-range interactions between optical solitons were almost impossible to control, generally leading to disorder. Here, we report that by tailoring weak, long-range soliton interactions of different origins, a large number of optical solitons in a mode-locked fiber laser could assemble into supramolecules with soliton-soliton spacing hundreds of times longer than the individual soliton duration. We demonstrate several remarkable features of these soliton supramolecules including flexibility, reversibility, constitutional diversity and dynamic stability, highlighting their potential applications in optical storage and computing, information transmission, and laser technology.

One Sentence Summary: Tailoring of weak, non-local soliton-soliton interactions allows the supramolecular assembly of optical temporal solitons in a mode-locked fiber laser.

Main Text: The concept of a supramolecule, describing an assembly of pre-existing components via weak interactions, is increasingly used in many disciplines (1-7). Different from chemical molecules formed via “strong” covalent bonds, the formation of supramolecular assemblies relies on non-covalent interactions whose “weak” nature causes several exotic features of such assemblies (1). The most remarkable ones are flexibility and reversibility which make the structures of supramolecules variable according to environmental perturbations, and these variations in structure are reversible (2-5). Another universal characteristic of supramolecules is their dynamic stability, which means that the individual components of a supramolecule robustly bind together, via weak interactions, to form a thermodynamically-stable state with a Gibbs energy lower than that of unassembled components (3-6). In practice, supramolecular assemblies persist long-term even when their internal structures were re-arranged, or the individual components were exchanged, incorporated or extruded (7). Moreover, the constitutional diversity of supramolecular assemblies allows large amounts of information to be stored, retrieved, and processed at the molecular level (4, 7).

Optical solitons, arising from an exact balance between nonlinear and dispersive effects, are analogous in many ways to particles. Individual optical solitons, when closely co-propagating, can strongly interact at their pulse tails, creating robust bound states that are frequently referred as soliton molecules or soliton crystals (8-13) in analogy to chemical molecules formed by strong covalent bonds. Supramolecular assemblies of optical solitons have,

however, escaped previous experimental observations. Weak, “non-covalent” interactions between optical solitons have been studied in a variety of systems (14-19). However, they have generally been regarded as either uncontrolled effects (15, 20, 21) or sources of noise leading to disordering of soliton streams during propagation (16, 22). In this paper, we show that by tailoring weak, long-range soliton interactions, a large amount of optical solitons in a mode-locked fiber laser cavity could assemble into stable, highly-ordered structures. We also observed in our experiments several key features of these supramolecular structures (1, 4) including flexibility, reversibility, diversity, and dynamic stability.

Weak, long-range soliton interactions

The supramolecular assembly of optical solitons demonstrated here involves two different types of long-range soliton interactions. As illustrated in Fig. 1, the global ordering of this assembly arises from optomechanical effects. In a simple case, a sequence of optical solitons, when its repetition rate is close to the resonant frequency of a mechanical oscillator (23), will coherently drive the oscillator through optical forces (see Fig. 1A). The mechanical motion of the moving mirror then acts back on the driving solitons by modulating their carrier frequencies (23). In a laser cavity, such optomechanical coupling can result in an optomechanical lattice whose period equals to that of the mechanical oscillation. This global lattice divides the laser cavity into many equally-spaced time-slots (24-27) within each of which multiple solitons can be trapped (see Fig. 1B).

Within each time-slot of the optomechanical lattice, the contactless binding of multiple solitons could be formed through a competition between effective forces of attraction and repulsion between the solitons. A long-range force of attraction arises from the optomechanical effect. In one time-slot of the lattice where two solitons are trapped (see Fig. 1C), the optically-driven mechanical oscillation can alter the carrier frequencies of the two solitons due to the energy transfer from the solitons to the moving mirror. The change in soliton frequency is directly related to the velocity of the mirror that the soliton experiences, and the frequency difference $\Delta\omega_a$ between the two solitons after passing through the mechanical oscillator can be expressed as

$$\Delta\omega_a = \frac{f_o \Delta t (v_1 - v_2)}{\hbar N}, \quad (1)$$

where f_o is the optical force exerted by one soliton on the mirror, Δt is the duration of the optical force exertion, \hbar is the reduced Planck constant, N is the photon number in one soliton, and v_1 and v_2 are the velocities of the mirror that the two solitons experience. When the two solitons propagate in optical fiber, this difference in their frequencies, acting in concert with fiber group-velocity dispersion (GVD), can result in a relative motion of the two solitons. Within an optical fiber with anomalous dispersion, a proper offset of the soliton repetition rate (lattice frequency) from the mechanical resonance frequency will result in a long-range force of attraction between these two solitons (see supplementary section S2.1).

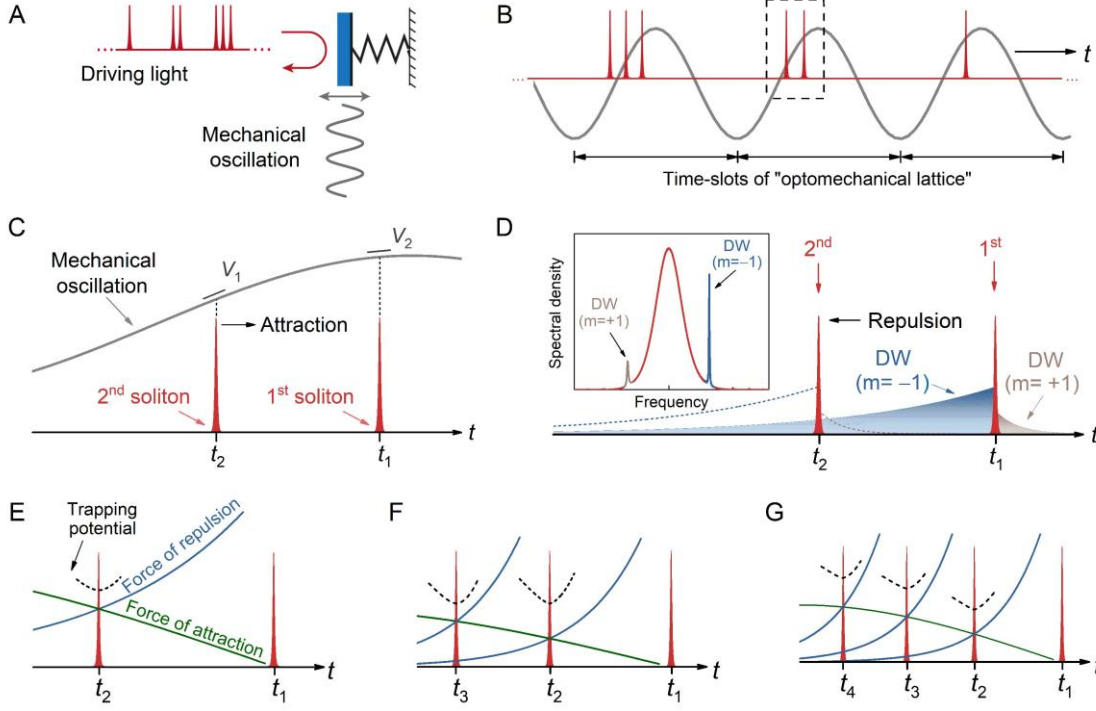


Fig. 1. Principle of a supramolecular assembly of optical solitons. (A) A sequence of contactlessly-bound solitons drives a mechanical oscillator when passing through it. (B) The optically-driven mechanical oscillation acts back on the driving solitons and varies their carrier frequencies, forming an effective “optomechanical lattice”. (C) Within one time-slot of the lattice, a long-range “force of attraction” between the two solitons arises due to the optomechanical effect. (D) The dispersive wave shed from the 1st soliton perturbs the 2nd soliton, resulting in a competing “force of repulsion” between the two solitons. The inset figure shows a typical soliton spectrum with asymmetric Kelly sidebands. (E) Competition between these two long-range “forces” of attraction and repulsion forms a temporal potential, trapping the 2nd soliton. (F) and (G) More solitons in such units can be stabilized by the build-up of additional trapping potentials.

A competing long-range force of repulsion between the two solitons will arise due to the long-lived dispersive waves shed by the solitons during propagation. The emission of dispersive waves, originating from periodic disturbances (28), is a generic phenomenon in both soliton transmission systems and soliton fiber lasers (28, 29). On the optical spectrum, dispersive waves appear as a series of narrow sidebands at several phase-matched frequencies (29), and in practice one ($m=-1$ order) sideband on the higher-frequency side usually dominates (see inset of Fig. 1D and supplementary section S4). In the time domain, this sideband corresponds to a long-lived, exponentially-decaying light wave (30), which, due to its slightly higher frequency, travels faster than the solitons in single-mode fiber with anomalous dispersion. The dominant dispersive wave that is shed from the 1st soliton eventually extends to the 2nd soliton during propagation (see Fig. 1D) and perturbs it through cross-phase modulation (31). This effect will also cause a frequency shift of the 2nd soliton which can be expressed as

$$\Delta\omega_d = \text{Im} \left[\int_{-\infty}^{+\infty} u_s^* \tanh(t / \tau_s) U_d dt \right] \delta z \quad (2)$$

(31), where u_s is the normalized temporal waveform of the perturbed (2nd) soliton, τ_s is the soliton duration, U_d is the temporal waveform of the dispersive wave shed from the 1st soliton, and δz is the propagation length of the perturbed soliton. With a proper phase relationship

between the dispersive wave and the perturbed soliton, an effective force of repulsion between the two solitons is exerted (see supplementary section S2.2), balancing the force of attraction as previously described.

The competition between these two long-range forces can create a temporal trapping potential for the 2nd soliton (see Fig. 1E), leading to a large, yet stabilized spacing between the two solitons. Therefore the two solitons trapped in one time-slot of the lattice contactlessly bind together through long-range soliton interactions, forming a robust unit. In principle, a third and even more solitons will also be stable in such units due to a similar contactless binding mechanism, which can be attributed to the formation of cascaded trapping potentials (see Fig. 1F and 1G).

Experimental set-up and results

Our experimental platform for demonstrating the supramolecular assembly of optical solitons is based on a mode-locked fiber laser, which is schematically illustrated in Fig. 2A (details in Fig. S1). A 2-m-long solid-core silica photonic crystal fiber (PCF), whose SEM photos are shown in Fig. 2B, was inserted in the fiber laser loop, providing the R₀₁ mechanical resonance at 1.887 GHz (32). By increasing pump power of the EDFA, a variety of soliton supramolecules could be generated and stably preserved over many minutes in this fiber laser cavity. All of these supramolecules have the same global ordering of optomechanical lattice whose period was locked with that of the PCF core resonance (23-27) which was 532 ps in practice. The cavity round-trip time was 85.12 ns, corresponding to 160 time-slots in the laser cavity divided by the optomechanical lattice.

In the experiments the duration of individual laser solitons was measured to be 670 fs (Fig. 2C), and a typical all-double-soliton (ADS) supramolecule with two contactlessly-bound solitons in all the time-slots of the lattice was measured using a 30-GHz photodetector. The time-domain trace of this ADS supramolecule was recorded using a 33-GHz oscilloscope, showing a perfect periodicity. The persistence-mode plot of the result is shown Fig. 2D with a time span equal to the period of the optomechanical lattice. As shown in Fig. 2D, the spacing between the two solitons in all the 160 time-slots is 90 ps which is more than 100 times longer than the individual soliton duration. The fast Fourier-transform (FFT) spectrum of the time-domain trace have sharp peaks at 1.881 GHz and its multiple harmonics (see Fig. 2E), indicating the global lattice of the structure. The modulation on the spectral envelope has a period of 11.1 GHz which agrees well with the 90-ps soliton spacing in each time-slot of the lattice. The existence of dispersive waves was verified by the sidebands observed on the laser spectrum (see Fig. 2F), and the phase locking between the soliton and the dispersive wave was indicated by the interferometric fringes which only appeared in the vicinity of the dominant sideband (see Fig. 2G and supplementary section S2.2). The period of the spectral fringe shown in Fig. 2G was 0.09 nm, also agreeing well with the 90-ps soliton spacing.

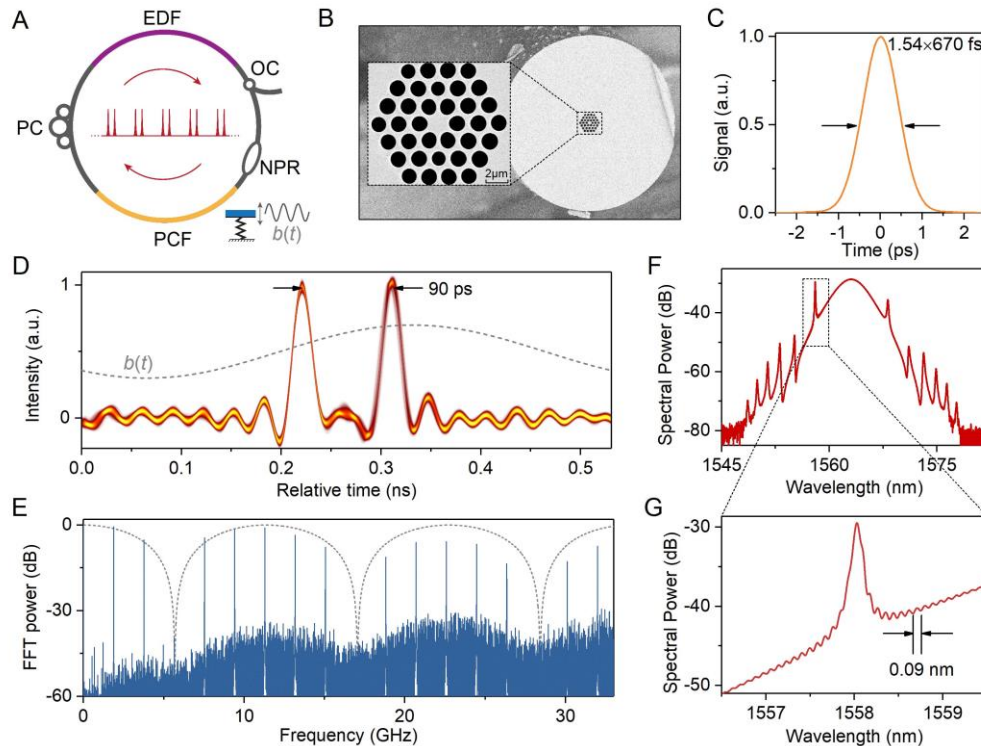


Fig. 2. Experimental set-up and a typical soliton supramolecule. (A) Schematic of the soliton fiber laser with a short piece of solid-core PCF used for providing a GHz-rate mechanical resonance, an erbium-doped fiber amplifier (EDFA), a polarization controllers (PC) for adjusting the light polarization state, an optical coupler (OC) for data recording, and a nonlinear polarization rotation (NPR) element for the laser self-start. (B) Scanning electronic microscopy (SEM) photos of the solid-core silica PCF used in the laser cavity. (C). Autocorrelation trace of the laser solitons. (D) Time-domain trace of the all-double-soliton (ADS) supramolecule, recorded using a fast oscilloscope working in persistence mode. The excited mechanical oscillation $b(t)$ is also plotted as the green dashed curve. (E) FFT power spectrum of the time-domain trace. The sinusoidal modulation on its envelope agrees well with the 90-ps soliton spacing. (F) Optical spectrum of the laser output, measured using an optical spectrum analyzer with 0.01 nm resolution. (G) Magnification of the optical spectrum near the dominant Kelly sideband, featuring interferometric fringes.

Flexibility and reversibility

In contrast to the “strong” covalent bonds in traditional soliton molecules, the “weak” nature of the long-range interactions in this system allows the soliton supramolecules able to rearrange their inner structures according to variations of external parameters. In practice, the spacing between the two solitons trapped in the time-slot of the ADS supramolecule could be continuously tuned back and forth over a range of tens of picoseconds, as the basic structure of the supramolecule was maintained. By introducing a tunable attenuator in the laser cavity (see Fig. S1), we could adjust the gain and loss of the laser cavity, leading to a continuous tuning of the dispersive wave intensity (see Fig. 3A and supplementary section S3.2). In the experiments we adjusted the dispersive wave intensity within a factor of three (see Fig. 3B), which dramatically varied the force of repulsion between the two solitons, leading to a continuous variation of the soliton spacing from 40 ps to 116 ps (see supplementary movie S1). We could also tuned the soliton spacing back and forth by varying the force of attraction between the two solitons. By adjusting the lattice frequency of the ADS supramolecule, which was accomplished by slightly adjusting the cavity length (see supplementary section S3.2) with respect to the

mechanical resonance frequency of the PCF, as shown in Fig. 3C, we could vary the amplitude of the mechanical vibration in the PCF core (25, 32). As shown in Fig. 3D, a tuning of the lattice frequency from 1.8725 GHz to 1.882 GHz led to a continuous decrease of the soliton spacing from 87 ps to 63 ps. Further increase of the lattice frequency led to a roll-over of the soliton spacing variation, agreeing well with the theoretical predictions in supplementary section S2.3. Structural flexibility and reversibility were also observed for the all-triple-soliton supramolecule generated in the same set-up. (See supplementary section S3.3 for details).

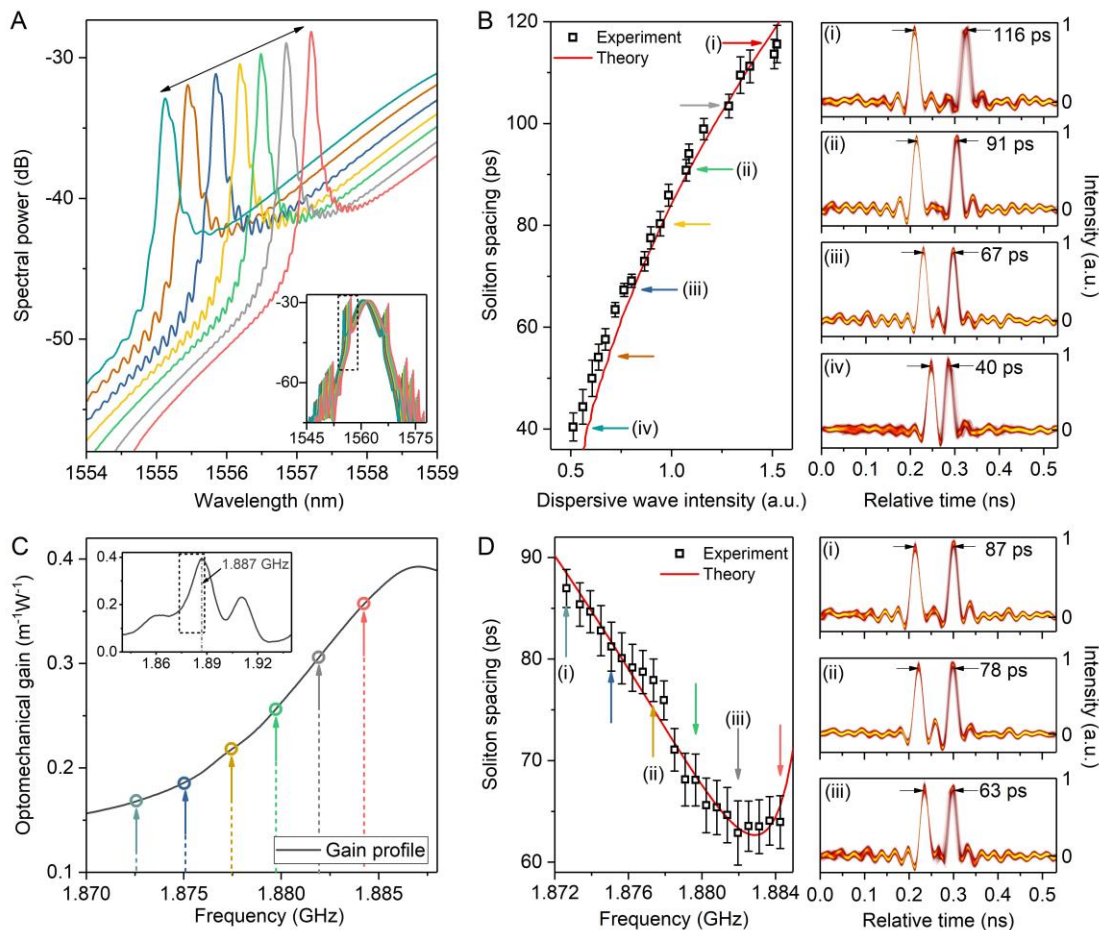


Fig. 3. Structural flexibility and reversibility of the ADS supramolecule. (A) Tailoring of the dispersive wave intensity, when the soliton bandwidth is invariant as shown in the inset. (B) Tuning of the soliton spacing through varying the intensity of the $m=-1$ order dispersive wave. The tuning range is from 40 ps to 116 ps, with four examples plotted in left columns (i) – (iv). (C) Tuning of the lattice frequency of the ADS supramolecule, implemented through adjusting the cavity length. The optomechanical gain band of the solid-core PCF is plotted as the inset, with a mechanical resonance frequency at 1.887 GHz. (D) Soliton spacing in all the double-soliton units decreases as the lattice frequency of the supramolecule is tuned toward the mechanical resonance frequency, which rolls over at ~ 1.882 GHz. The tuning range of the soliton spacing is from 63 ps to 87 ps, with three examples plotted in left columns (i) – (iii). The experimental data are plotted as black squares in (B) and (D), which agree well with the red theory curves fitted using Eq. (S13) in supplementary section S2.3.

Constitutional diversity and dynamic stability

The maximum number of solitons that can be trapped in one time-slot of the optomechanical lattice is mainly limited by the ratio between the period of the lattice and the internal soliton spacing. The number of time-slots in the soliton supramolecule is determined by both the

resonance frequency of the mechanical oscillator and the cavity round-trip time. The maximum time-slot number achieved in our experiments was more than one thousand, which was obtained in a longer laser cavity with 350 ns round-trip time using a piece of PCF with the R₀₁ mechanical core resonance at 2.83 GHz. If the parameters of laser cavity and PCF were maintained, the pump power of the EDFA limits in practice the maximum number of the assembled solitons in the supramolecule which is around 520 in our current set-up shown in Fig. S1.

Using the set-up shown in Fig. S1, we generated a stable all-triple-soliton supramolecule (Fig. 4A) and a variety of hybrid supramolecules composed of different bound-soliton units with maximum of four solitons trapped in the time-slots of the optomechanical lattice. Fig. 4B illustrates one example of the hybrid supramolecule composed of quadruple-soliton units in several time-slots and triple-soliton units in the rest. We show two more examples in supplementary section S5. In these soliton supramolecules, five possible types of bound-soliton units with 0–4 solitons in them could coexist and stably propagate in the fiber laser loop, while the relative positions of the units in the laser cavity were fixed by the optomechanical lattice. At this stage, the soliton numbers in the time-slots were arbitrary and uncontrolled (the formation process of these supramolecular assemblies is briefly discussed in supplementary section S1 and S5). Independent control of the soliton number in each time-slot should be possible, if the previously-developed technique was used (23).

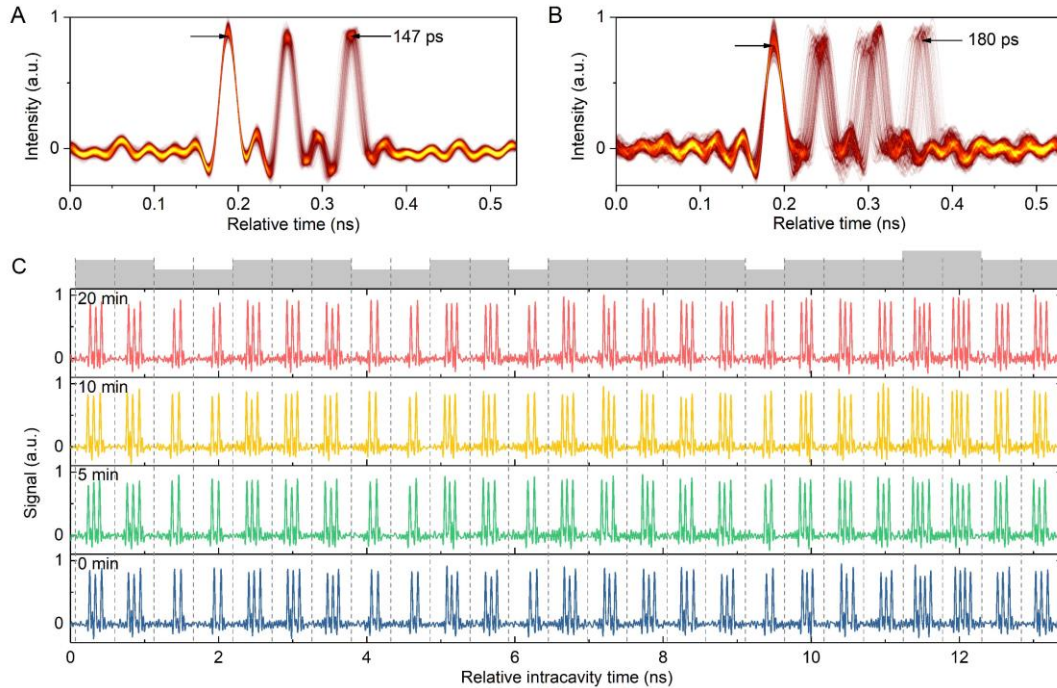


Fig. 4. Constitutional diversity and dynamic stability of the supramolecular assemblies. (A) Stable all-triple-soliton supramolecule, recorded using OSC working in persistence mode. (B) A typical hybrid soliton supramolecule with three solitons or four solitons contactlessly-bound in different time-slots of the optomechanical lattice. (C) Long-term preservation of a hybrid soliton supramolecule composed of double-, triple-, and quadruple-soliton units. Recording was performed every 5 min over 20 min. Data in only 25 consecutive time-slots are plotted due to the limited space, and the dashed lines indicate the time-slots of the optomechanical lattice.

In the laboratory all these supramolecular assemblies of optical solitons, when formed, show excellent dynamic stability. Without deliberate perturbations, they can be stably preserved in this freely-running fiber laser cavity over many minutes. In the experiments we performed a

20-min-long recording of a typical hybrid soliton supramolecule which was composed of double-, triple- and quadruple-soliton units. The results shown in Fig. 4C exhibit an robust preservation of this soliton supramolecule over the recording time, corresponding to an error-free transmission of this assembled soliton sequence in this fiber laser loop over one-fifth of a billion kilometers (longer than an astronomical unit).

Discussion

Our current experiments demonstrated the concept of supramolecular assembly of optical temporal solitons with simple examples of these assemblies. The observed soliton supramolecules have shown structural complexity of hierarchy: The optomechanical lattice provides the period of global ordering which is hundreds of picoseconds, while contactless binding of solitons in each time-slot of the lattice provides the local spacing which is tens of picoseconds. The fundamental components structuring the supramolecules demonstrated here are, however, individual optical solitons. Supramolecular assemblies of a variety of optical components including individual optical soliton and a variety of soliton molecules might be possible. Such assemblies, relying on more diverse and complicated long-range interactions of soliton-soliton, soliton-molecule or molecule-molecule, would possibly extend the constitutional diversity and componential recognition of such soliton supramolecules (5-7).

The supramolecular features of the optical soliton assemblies are responsible for several of their potential applications. The diversity and flexibility of the supramolecular structures allow the possibility of coded soliton supramolecules for storage, replication and logic operations of optical information in analog to molecular computing (5, 33) and molecular machine (6, 34) in supramolecular chemistry and biology. Remarkably, in comparison with traditional soliton storage and transmission systems which generally have binary formats (23, 35, 36), the soliton supramolecules demonstrated here, on one hand, resemble closely some biological or chemical systems that are capable of molecule-level storages of information (7). In each unit of a soliton supramolecule, several diverse states containing 0 to M solitons can exist, extending the data capacity of such supramolecule to M^N , where N is the total number of units. On the other hand, different from chemical or biological supramolecules which are generally static assemblies of real particles, the soliton supramolecules demonstrated here are composed of optical temporal solitons which, analogous to particles in a certain sense, are essentially light waves propagating in a nonlinear medium (11, 35). The dynamic stability of these soliton supramolecules allows the robust propagation of assembled soliton sequences over ultra-long distance, which might be potentially used for repeater-less (optical-to-electrical converter free) transmission of information (35). In the field of laser technology, the supramolecular assembly of optical solitons in the laser cavity shows structural diversity and flexibility that make it feasible to construct waveform-programmable lasers (13), and the responsiveness of the supramolecular structures to variations of environmental parameters paves the way to environment-adaptive lasers and laser sensing applications.

References:

1. R. F. Service, P. Szuromi, J. Uppenbrink, Strength in numbers. *Science* **295**, 2395-2395 (2002).
2. P. W. K. Rothmund, Folding DNA to create nanoscale shapes and patterns. *Nature* **440**, 297-302 (2006).

3. T. Kato, Self-assembly of phase-segregated liquid crystal structures. *Science* **295**, 2414-2418 (2002).
4. G. M. Whitesides, B. Grzybowski, Self-assembly at all scales. *Science* **295**, 2418-2421 (2002).
5. D. N. Reinhoudt, M. Crego-Calama, Synthesis beyond the molecule. *Science* **295**, 2403-2407 (2002).
6. E. Mattia, S. Otto, Supramolecular systems chemistry. *Nat. Nanotech.* **10**, 111-119 (2015).
7. J.-M. Lehn, Toward self-organization and complex matter. *Science* **295**, 2400-2403 (2002).
8. B. A. Malomed, Bound solitons in the nonlinear Schrödinger-Ginzburg-Landau equation. *Phys. Rev. A* **44**, 6954-6957 (1991).
9. N. N. Akhmediev, A. Ankiewicz, J. M. Soto-Crespo, Multisoliton Solutions of the Complex Ginzburg-Landau Equation. *Phys. Rev. Lett.* **79**, 4047-4051 (1997).
10. M. Stratmann, T. Pagel, F. Mitschke, Experimental Observation of Temporal Soliton Molecules. *Phys. Rev. Lett.* **95**, 143902 (2005).
11. P. Grelu, N. Akhmediev, Dissipative solitons for mode-locked lasers. *Nat. Photon.* **6**, 84-92 (2012).
12. G. Herink, F. Kurtz, B. Jalali, D. R. Solli, C. Ropers, Real-time spectral interferometry probes the internal dynamics of femtosecond soliton molecules. *Science* **356**, 50-54 (2017).
13. D. C. Cole, E. S. Lamb, P. Del'Haye, S. A. Diddams, S. B. Papp, Soliton crystals in Kerr resonators. *Nat. Photon.* **11**, 671-676 (2017).
14. E. M. Dianov, A. V. Luchnikov, A. N. Pilipetskii, A. N. Starodumov, Electrostriction mechanism of soliton interaction in optical fibers. *Opt. Lett.* **15**, 314-316 (1990).
15. K. Smith, L. F. Mollenauer, Experimental observation of soliton interaction over long fiber paths: discovery of a long-range interaction. *Opt. Lett.* **14**, 1284-1286 (1989).
16. J. K. Jang, M. Erkintalo, S. G. Murdoch, S. Coen, Ultraweak long-range interactions of solitons observed over astronomical distances. *Nat. Photon.* **7**, 657-663 (2013).
17. D. Y. Tang, W. S. Man, H. Y. Tam, P. D. Drummond, Observation of bound states of solitons in a passively mode-locked fiber laser. *Phys. Rev. A* **64**, 033814 (2001).
18. C. Rotschild, B. Alfassi, O. Cohen, M. Segev, Long-range interactions between optical solitons. *Nat. Phys.* **2**, 769-774 (2006).
19. R. Weill, A. Bekker, V. Smulakovsky, B. Fischer, O. Gat, Noise-mediated Casimir-like pulse interaction mechanism in lasers. *Optica* **3**, 189-192 (2016).
20. R. P. Davey, N. Langford, A. I. Ferguson, Interacting solitons in erbium fibre laser. *Electron. Lett.* **27**, 1257-1259 (1991).
21. Y. Wang *et al.*, Universal mechanism for the binding of temporal cavity solitons. *Optica* **4**, 855-863 (2017).
22. L. Socci, M. Romagnoli, Long-range soliton interactions in periodically amplified fiber links. *J. Opt. Soc. Am. B* **16**, 12-17 (1999).
23. M. Pang, W. He, X. Jiang, P. St.J. Russell, All-optical bit storage in a fibre laser by optomechanically bound states of solitons. *Nat. Photon.* **10**, 454-458 (2016).
24. M. Pang *et al.*, Stable subpicosecond soliton fiber laser passively mode-locked by gigahertz acoustic resonance in photonic crystal fiber core. *Optica* **2**, 339-342 (2015).

25. W. He, M. Pang, P. St.J. Russell, Wideband-tunable soliton fiber laser mode-locked at 1.88 GHz by optoacoustic interactions in solid-core PCF. *Opt. Express* **23**, 24945-24954 (2015).
26. M. Pang, W. He, P. St.J. Russell, Gigahertz-repetition-rate Tm-doped fiber laser passively mode-locked by optoacoustic effects in nanobore photonic crystal fiber. *Opt. Lett.* **41**, 4601-4604 (2016).
27. W. He, M. Pang, C. R. Menyuk, P. St.J. Russell, Sub-100-fs 1.87 GHz mode-locked fiber laser using stretched-soliton effects. *Optica* **3**, 1366-1372 (2016).
28. S. M. J. Kelly, Characteristic sideband instability of periodically amplified average soliton. *Electron. Lett.* **28**, 806-807 (1992).
29. D. U. Noske, N. Pandit, J. R. Taylor, Source of spectral and temporal instability in soliton fiber lasers. *Opt. Lett.* **17**, 1515-1517 (1992).
30. J. P. Gordon, Dispersive perturbations of solitons of the nonlinear Schrödinger equation. *J. Opt. Soc. Am. B* **9**, 91-97 (1992).
31. A. Bondeson, M. Lisak, D. Anderson, Soliton Perturbations: A Variational Principle for the Soliton Parameters. *Phys. Scripta* **20**, 479 (1979).
32. M. S. Kang, A. Nazarkin, A. Brenn, P. St.J. Russell, Tightly trapped acoustic phonons in photonic crystal fibres as highly nonlinear artificial Raman oscillators. *Nat. Phys.* **5**, 276-280 (2009).
33. L. M. Adleman, Molecular computation of solutions to combinatorial problems. *Science* **266**, 1021-1024 (1994).
34. V. Balzani, A. Credi, F. M. Raymo, J. F. Stoddart, Artificial molecular machines. *Angew. Chem. Int. Ed.* **39**, 3348-3391 (2000).
35. H. A. Haus, W. S. Wong, Solitons in optical communications. *Rev. of Mod. Phys.* **68**, 423-444 (1996).
36. F. Leo *et al.*, Temporal cavity solitons in one-dimensional Kerr media as bits in an all-optical buffer. *Nat. Photon.* **4**, 471-476 (2010).
37. L. E. Nelson, D. J. Jones, K. Tamura, H. A. Haus, E. P. Ippen, Ultrashort-pulse fiber ring lasers. *Appl. Phys. B* **65**, 277-294 (1997).
38. M. Hofer, M. E. Fermann, F. Haberl, M. H. Ober, A. J. Schmidt, Mode-locking with cross-phase and self-phase modulation. *Opt. Lett.* **16**, 502-504 (1991).
39. A. N. Pilipetskii, E. A. Golovchenko, C. R. Menyuk, Acoustic effect in passively mode-locked fiber ring lasers. *Opt. Lett.* **20**, 907-909 (1995).
40. M. L. Dennis, I. N. Duling III, Experimental study of sideband generation in femtosecond fiber lasers. *IEEE J. Quantum Electron.* **30**, 1469-1477 (1994).
41. P. M. Becker, A. A. Olsson, J. R. Simpson, Erbium-doped fiber amplifiers: fundamentals and technology, *Academic Press* (1999).

Supplementary Materials:

Section S1-S5

Figures S1-S9

Movies S1

Supplementary Materials for
Supramolecular assembly of optical solitons via long-range interactions

W. He, M. Pang, J. Huang, C. R. Menyuk, P. St.J. Russell

Correspondence to: meng.pang@mpl.mpg.de

This PDF file includes:

Supplementary Text Section S1 to S5
Figs. S1 to S9
Captions for Movies S1

Other Supplementary Materials for this manuscript includes the following:

Movies S1

Supplementary Text

S1. Experimental and diagnostic set-up

The platform used to perform the experiments was a soliton fiber laser with a ring configuration. The experimental set-up is shown in Fig. S1. A 2-m-long solid-core silica photonic crystal fiber (PCF) was spliced into the laser cavity with an insertion loss of ~ 1.7 dB. The PCF had a core diameter of $1.95 \mu\text{m}$, with R_{01} mechanical core resonance at 1.887 GHz (32). Multiple pulses in the laser cavity could be harmonically mode-locked to this GHz-rate mechanical core resonance in the PCF (23-25). The laser gain medium was a 1.2-m length of erbium-doped fiber (EDF) with 110 dB/m peak absorption at 1530 nm. Two pump laser diodes (LD-1 and LD-2) provided a maximum combined pump power of ~ 1.6 W at 976 nm. Two polarization controllers (PC-1 and PC-3 in Fig. S1) and a polarizer were used to configure a fast saturable absorber, enabling the self-starting of mode-locking (24). Another polarization controller (PC-2) before the PCF was used to adjust the polarization state of light launched into the PCF. A tunable delay line was used to adjust the cavity length, and a tunable attenuator to adjust the cavity loss. An optical isolator (ISO) ensured the unidirectional operation of the laser.

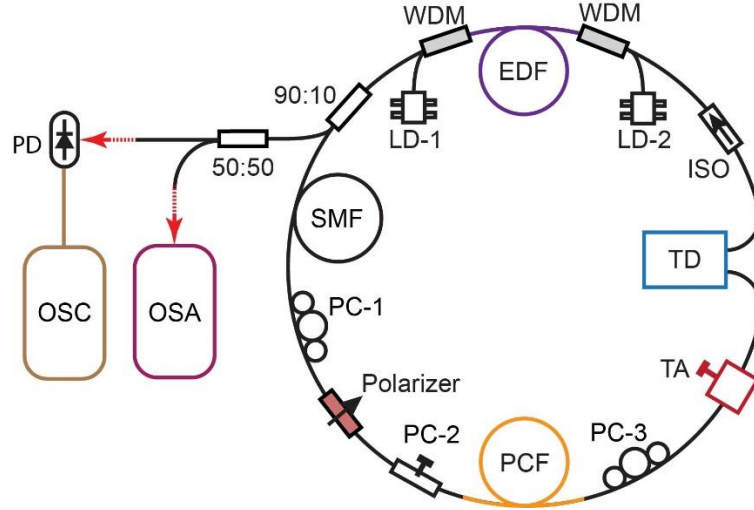


Fig. S1. Experimental and diagnostic set-up. A unidirectional fiber laser cavity is operated in the soliton regime, and the laser output was recorded using a fast oscilloscope (OSC) and a high-resolution optical spectrum analyzer (OSA). EDF: Erbium-doped fiber; WDM: wavelength division multiplexer; LD: laser diode; SMF: single-mode fiber; PC: polarization controller; PCF: photonic crystal fiber; TA: tunable attenuator; TD: tunable delay line; ISO: optical isolator; PD: photo detector.

The total cavity length was ~ 17 m, corresponding to a cavity free spectral range (FSR) of ~ 11.7 MHz. The EDF had a normal dispersion of $+0.077 \text{ ps}^2/\text{m}$ at 1550 nm, the PCF had an anomalous dispersion of $-0.157 \text{ ps}^2/\text{m}$, and the rest of the cavity was made from conventional single-mode fiber (SMF) with a length of ~ 13 m and an anomalous dispersion of $-0.0225 \text{ ps}^2/\text{m}$. The cavity average dispersion was calculated to be $-0.046 \text{ ps}^2/\text{m}$, ensuring operation of this laser in the soliton regime (37). The cavity loss could be tuned from ~ 6 dB to >30 dB by adjusting the intra-cavity tunable attenuator (TA) with a resolution of 0.02 dB. The laser cavity length could be varied using an intra-cavity tunable delay line (TD) with a tuning range of 0.15 m and a resolution of $3 \mu\text{m}$.

When the laser was harmonically mode-locked by the optomechanical effect in the PCF, the cavity round-trip time was effectively divided into 160 time-slots by the optically-driven GHz-

rate mechanical vibration in the PCF core, providing an effective optomechanical lattice. Within each time-slot (mechanical vibration cycle) of the lattice, one unit containing several contactlessly-bound solitons could be trapped long-term. Both the self-starting process and stable operation of this soliton fiber laser rely on the effect of nonlinear polarization rotation (NPR) (38). For steady operation of this mode-locked laser, a proper working point of the NPR could be achieved through fine adjustments of PC-1 and PC-3 in the laser cavity. This working point ensured, on one hand, a fast saturable absorber effect at low optical intensities, suppressing the build-up of background noise. On the other hand, the NPR effect also provided a fast saturable gain, such that at higher optical intensities, the optical loss becomes higher in the cavity, ensuring that all pulses in the cavity have almost the same intensity (23). In the experiments both the self-starting of the laser and the fine structure of the stationary soliton supramolecule depended critically on manual adjustments of the PCs. However, after we set a proper working point of the NPR effect, no further adjustment of the PCs is required for long-term preservation of the soliton supramolecule.

In the diagnostic set-up, the laser output was detected using a 30-GHz photodetector, and the electrical signal from the detector was recorded using a 33-GHz oscilloscope (OSC). The response time of this real-time detection is ~ 20 ps which sets the pulse width shown in all the plots that were recorded using the OSC. The timing jitter of the OSC in sampling is ~ 2 ps which gives the measurement error in reading fine structures of the supramolecules. For measuring the actual duration of laser solitons, a second-harmonic autocorrelator was used with a time resolution of 20 fs. Before the autocorrelator, a 0.9 m length fiber with normal dispersion of $0.055 \text{ ps}^2/\text{m}$ at 1550 nm was used to compensate for the anomalous dispersion of the 2-m-long SMF28 fiber patch cord at the laser output port. The optical spectrum of the laser output was measured using an optical spectrum analyzer with a resolution of 0.01 nm.

S2. Long-range forces between optical solitons: Theory

We present here the theoretical model for studying the long-range soliton-soliton interactions. We consider the all-double-soliton (ADS) supramolecule which is composed of double-soliton units in all the time-slots of the optomechanical lattice (see Fig. 2D). In a frame moving with the reference soliton (the 1st soliton in Fig. S2), the 1st soliton is located at t_1 and the 2nd soliton is located at t_2 , with a spacing $\Delta t = t_1 - t_2$. The effective force of attraction between the two solitons results in a slower group velocity of the 2nd soliton, which delays the 2nd soliton relative to the 1st one during propagation. Conversely, a faster velocity of the 2nd soliton would result from an effective force of repulsion. When the soliton spacing is hundreds of times longer than the duration of the individual soliton, soliton interactions become long-range and thus distinct from direct soliton interactions through the overlap of soliton tails in traditional soliton molecules (8-11). The existence of such long-range soliton interactions relies on some long-lived process that links multiple solitons that are located far from each other.

S2.1. Force of attraction due to the optomechanical effect in the PCF

When the ADS supramolecule circulates in the laser cavity with a lattice frequency of Ω_a , it coherently drives the mechanical core resonance in the PCF. The optically-driven mechanical vibration, in the form of a refractive index modulation, acts back on the driving solitons by varying their carrier frequencies. In practice, we only consider the LP₀₁ optical mode and the R₀₁ mechanical resonance in the PCF core, since the PCF used in our experiments was designed for guiding only this fundamental optical mode with low loss, and the R₀₁ mechanical mode has the

largest overlap integral with the LP₀₁ optical mode (32). The R₀₁ mechanical mode in the PCF has a resonant frequency of Ω_{01} and a mechanical bandwidth of Γ_B . In a reference frame moving with the soliton supramolecule, the mechanical vibration in the PCF core driven by the ADS supramolecule can be expressed as (23):

$$b(t) = \frac{\gamma_e |Q| P_{av} \cos(\Omega_a \Delta t / 2)}{2\pi c n_0 A_{eff} \Omega_a \sqrt{4\delta_\Omega^2 + \Gamma_B^2}} \sin(\Omega_a t), \quad (S1)$$

where $b(t)$ is the material density variation as a function of time, γ_e is the electrostrictive constant of silica, c is the speed of light in vacuum, n_0 is the refractive index of silica, A_{eff} is the effective mode area of LP₀₁ optical mode, δ the frequency off-set ($\delta_\Omega = \Omega_a - \Omega_{01}$), and P_{av} is the average optical power in the PCF. The overlap integral Q is defined as $Q = \langle \rho_{01} \nabla_\perp^2 |E_{01}|^2 \rangle / \langle \rho_{01}^2 \rangle$, where ρ_{01} and E_{01} are the transverse field distributions of the R₀₁ mechanical mode and the LP₀₁ optical mode. The timing of the double-soliton unit relative to the excited mechanical vibration in one time-slot can be expressed using

$$t_e = \frac{1}{\Omega_a} \tan^{-1} \left(-\frac{2\delta_\Omega}{\Gamma_B} \right), \quad (S2)$$

where t_e is the equivalent driving center of the double-soliton unit, and the timing of the 1st and the 2nd solitons in this frame can be expressed as $t_1 = t_e + \Delta t/2$ and $t_2 = t_e - \Delta t/2$.

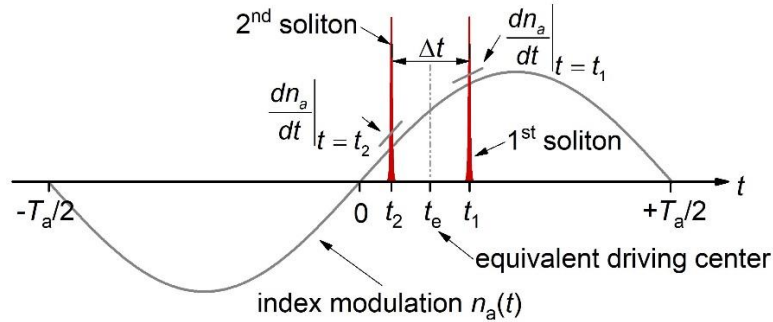


Fig. S2. One double-soliton unit of the ADS supramolecule and the optically-driven index modulation within one time-slot of the optomechanical lattice. In one time-slot, two solitons locate at t_1 and t_2 , giving a soliton spacing of Δt and an equivalent driving center of t_e . When propagating in the PCF core, the two solitons experience different refractive index slopes.

The optically-driven mechanical vibration modulates the effective refractive index of the LP₀₁ optical mode through the stress-optical effect, expressed as

$$n_a(t) = \frac{\gamma_e \Theta}{2n_0 \rho_0} b(t) = C_a \frac{P_{av}}{\Omega_a \sqrt{4\delta_\Omega^2 + \Gamma_B^2}} \cos\left(\frac{\Omega_a \Delta t}{2}\right) \sin(\Omega_a t), \quad (S3a)$$

$$C_a = \frac{\gamma_e^2 |Q| \Theta}{4\pi c n_0^2 A_{eff} \rho_0}, \quad (S3b)$$

where ρ_0 is the material density of silica, and Θ is the overlap integral between the normalized intensity field of the LP₀₁ optical mode and the normalized density field of the R₀₁ mechanical mode, defined as $\Theta = \langle \rho_{01} |E_{01}|^2 \rangle / \langle \rho_{01}^2 \rangle$.

Back-action of the mechanical vibration results in a carrier frequency shift of the driving soliton, which is directly related to the refractive index slope that the soliton experiences as (39):

$$\frac{\partial \omega_s}{\partial z} = -\frac{\omega_s}{c} \frac{\partial n_a}{\partial t}, \quad (\text{S4})$$

where ω_s is the soliton carrier frequency. As shown in Fig. S2, in one mechanical cycle, the two solitons experience different index slopes, leading to a carrier frequency difference between the two solitons. Using Eq. (S3) and Eq. (S4), this frequency difference after a single-trip propagation in the PCF can be expressed as:

$$\Delta \omega_a = \delta \omega_{s2} - \delta \omega_{s1} = \frac{2C_a \omega_s P_{av} L_{PCF}}{c} \frac{\delta_\Omega}{4\delta_\Omega^2 + \Gamma_B^2} \sin(\Omega_a \Delta t), \quad (\text{S5})$$

where $\delta \omega_{s1}$ and $\delta \omega_{s2}$ are the carrier frequency shifts of the 1st and 2nd solitons due to the optomechanical effect in the PCF, and L_{PCF} is the PCF length. When the lattice frequency of the soliton supramolecule is lower than the mechanical resonance frequency in the PCF ($\delta_\Omega < 0$), $\Delta \omega_a$ remains negative, which means that the optomechanical effect leads to a lower carrier frequency of the 2nd soliton than that of the 1st one. In a fiber cavity with anomalous average dispersion, solitons with lower frequency propagate at a lower group velocity, which delays the 2nd soliton relative to the 1st soliton during propagation, leading to an effective force of attraction between the two solitons.

S2.2. Force of repulsion due to dispersive wave perturbations

A competing long-range interaction between solitons results from the dispersive waves that are shed from one soliton and extend in the time domain to the neighboring solitons and perturb them through cross-phase modulation (31). Dispersive waves, which corresponds to Kelly sidebands in soliton fiber lasers, appear at discrete frequencies on the soliton spectrum (Fig. S3A). In the systems for long-distance soliton transmission and soliton fiber lasers, the existence of dispersive waves is a generic phenomenon that is due to periodic disturbances arising from the discrete dispersion, nonlinearity, gain and loss in these systems (28, 29). During propagation, optical solitons coherently transfer their energy to several discrete frequency components (sidebands). Due to gain filtering in the EDFA, those sidebands would always experience a net loss in the cavity, since their frequencies deviate from the central frequency of the soliton where the maximum gain in the EDFA equals the total cavity loss. During one cavity round-trip, the nonlinear gain of the sidebands balances their net cavity loss due to energy conversion from solitons to sidebands, determining the stationary intensities of the sidebands. In practice, due to the asymmetric gain profile in the EDFA and higher-order dispersion in the fiber cavity, these Kelly sidebands are usually asymmetrically distributed on the soliton spectrum (40). The situation we consider in the main text is that the $m=-1$ order sideband has the highest intensity as shown in Fig. S3A (Other possibilities are demonstrated in section S4)

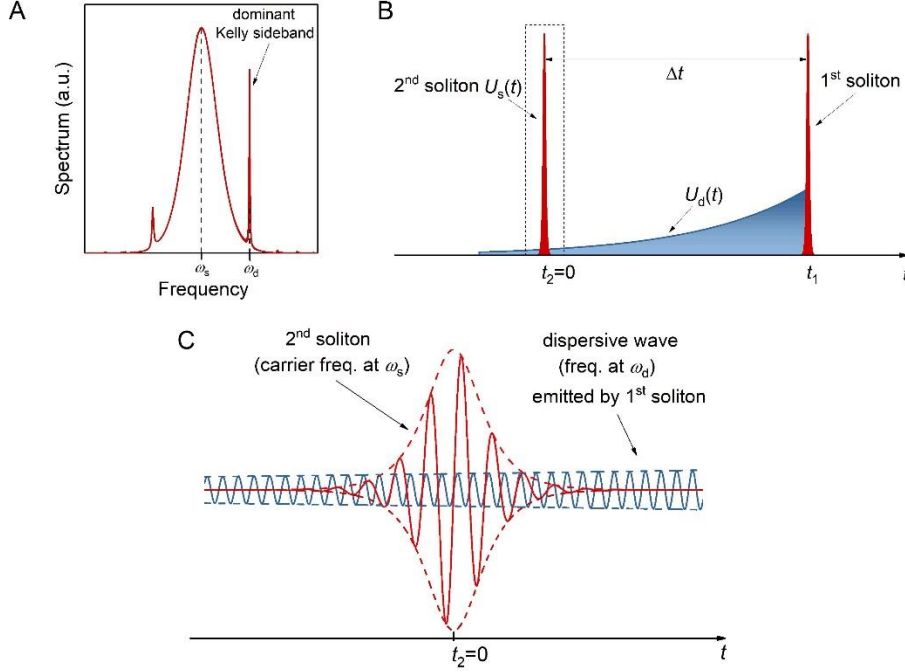


Fig. S3. Long-range soliton interactions due to dispersive wave perturbations. (A). Typical soliton spectrum with a dominant ($m=-1$ order) Kelly sideband at ω_d . (B) This dominant sideband corresponds, in the time domain, to dispersive waves. The dispersive waves shed from the 1st soliton has a faster group velocity than the soliton, and extends to the 2nd soliton. (C) Interactions between the 2nd soliton and the dispersive wave shed from the 1st soliton shift the carrier frequency of the 2nd soliton.

This dominant sideband corresponds, in the time domain, to a packet of dispersive waves shed from solitons in the laser cavity. Within one double-soliton unit, the dispersive wave shed from the 1st soliton (see Fig. S3B) travels faster than solitons due to its higher carrier frequency, and its exponentially-decaying envelope is due to the net cavity-loss that it experiences in the cavity. In a reference frame moving with the 2nd soliton ($t_2 = 0$), the dispersive waves shed from the 1st soliton can be expressed as:

$$U_d(t) = A_d \exp[h(t - \Delta t)] \exp[i\omega_d(t - \Delta t) - i\varphi_d(z)], \quad (S6)$$

where A_d is the amplitude, h is the decay rate, ω_d is the carrier frequency, and $\varphi_d(z)$ is the phase of the dispersive wave. Note that $\varphi_d(z)$ includes the propagation term of the dispersive wave, and varies as the wave propagates in the cavity. In practice, while A_d and ω_d could be estimated using peak intensity and central frequency of the dominant sideband, h could be calculated using the bandwidth of the sideband.

In this moving frame, the 2nd soliton can be expressed as

$$U_s(t) = A_s u_s(t) = A_s \operatorname{sech}[t/\tau_s] \exp[i\omega_s t - i\varphi_s(z)], \quad (S7)$$

where A_s is the amplitude, $u_s(t)$ the normalized profile, τ_s the pulse width, and φ_d the phase of the 2nd soliton varying with propagation length. According to soliton perturbation theory (31), the carrier frequency of the 2nd soliton varies due to the dispersive wave shed from the 1st soliton (see Fig. S3C) following the expression

$$\frac{d\omega_s}{dz} = \text{Im} \left\{ \int_{-\infty}^{+\infty} u_s^*(t) \tanh(t/\tau_s) U_d(t) dt \right\}, \quad (\text{S8})$$

where the operator $\text{Im}\{\}$ stands for the imaginary part. By substituting Eq. (S6) and Eq. (S7) into Eq. (S8), we can obtain

$$\frac{d\omega_s}{dz} = B(\Delta\omega) A_d \exp(-h\Delta t) \cos[\Delta\varphi(z)], \quad (\text{S9a})$$

$$\begin{aligned} B(\Delta\omega) &= \int_{-\infty}^{+\infty} \text{sech}(t/\tau_s) \tanh(t/\tau_s) \sin(\Delta\omega t) dt \\ &= \pi\Delta\omega\tau_s \text{sech}(\pi\Delta\omega\tau_s/2), \end{aligned} \quad (\text{S9b})$$

where $\Delta\omega = \omega_d - \omega_s$ is the carrier frequency difference, and $\Delta\varphi(z) = \varphi_s(z) - \varphi_d(z)$ is the phase difference between the soliton and the dispersive wave. In practice, $B(\Delta\omega)$ is a constant close to 1, and the accumulated frequency shift of the 2nd soliton after each cavity round-trip (RT) can be expressed as:

$$\Delta\omega_d^{\text{RT}} = A_d B(\Delta\omega) \exp(-h\Delta t) \int_{z_0}^{z_0+L_c} \cos[\Delta\varphi(z)] dz, \quad (\text{S10})$$

where z_0 is the starting point for integral in the cavity, and L_c the cavity length. Note that in Eq. (S10) we assume a uniform intensity distribution of the dispersive wave over the cavity. Otherwise we would have to include an intensity distribution $A_d(z)$ within the integral.

The phase-matching condition for dispersive wave generations (29) requires that the accumulated phase difference between solitons and dispersive waves over one cavity round-trip should be integer multiples of 2π . For the $m=-1$ order dispersive wave, this accumulated phase difference should be -2π (29). If we define the phase difference at an arbitrary position (z_0) in the cavity as $\Delta\varphi_0$, we obtain:

$$\Delta\varphi(z) = \int_{z_0}^z \left[\frac{1}{2} \beta_2(z) \Delta\omega^2 - \frac{1}{2} \gamma(z) |A_s(z)|^2 \right] dz + \Delta\varphi_0, \quad (\text{S11a})$$

$$\Delta\varphi(z + L_c) - \Delta\varphi(z) = -2\pi, \quad (\text{S11b})$$

where $\beta_2(z)$ and $\gamma(z)$ are the dispersion and nonlinearity maps of the laser cavity. By substituting Eq. (S11a) into Eq. (S10), we can obtain:

$$\Delta\omega_d^{\text{RT}} = A_d B(\Delta\omega) \exp(-h\Delta t) \psi(\Delta\varphi_0), \quad (\text{S12a})$$

$$\psi(\Delta\varphi_0) = \int_{z_0}^{z_0+L_c} \cos \left\{ \int_{z_0}^z \left[\frac{1}{2} \beta_2(z) \Delta\omega^2 - \frac{1}{2} \gamma(z) |A_s(z)|^2 \right] dz + \Delta\varphi_0 \right\} dz. \quad (\text{S12b})$$

Using Eq. (S12b), it can be seen that when both the dispersion and nonlinearity distributions in the cavity are fixed, the integral ψ only depends on the initial phase difference ($\Delta\varphi_0$), which determines the sign of the carrier frequency shift of the perturbed soliton. In order to form stable double-soliton units, an effective force of repulsion due to this dispersive wave perturbation is necessary to balance the force of attraction due to the optomechanical effect. According to Eq. (S12), this requires a special phase relationship between the dispersive wave shed from the 1st soliton and the 2nd soliton, which ensures a positive $\Delta\omega_d^{\text{RT}}$. Acting in concert with the anomalous average dispersion of the laser cavity, this positive $\Delta\omega_d^{\text{RT}}$ would lead to a faster group velocity of the 2nd soliton than that of the 1st one, resulting in an effective force of repulsion between the two solitons. The existence of this phase relationship has been verified in the experiments. As shown

in Fig. 2G and Fig. 3A in the main text, we observed clear interferometric fringes on the laser spectra, which appeared only in the vicinity of the dominant sideband, indicating the phase locking between the dispersive wave and the soliton.

We observed in the experiments that the interferometric fringes and the corresponding phase locking were very robust over time. This stable phase locking might be attributed to the nonlinear coupling between the dispersive wave and the perturbed soliton. The concept of attractor in a nonlinear system might be introduced to investigate the robustness of this phase locking between the two optical waves. At present, we use this phase relation as a basic assumption of the theoretical derivation, and leave a full explanation of its origin as an open question.

S2.3. Balance of the two long-range forces

The build-up of the contactless binding of the two solitons in one time-slot is based on a perfect balance between the effective long-range forces of attraction and repulsion. Over each cavity round-trip, the overall carrier frequency shift of the 2nd soliton relative to the 1st soliton should equal to zero ($\Delta\omega_a + \Delta\omega_d^{\text{RT}} = 0$). Therefore the two solitons always have the same group velocity during propagation and travel together with an invariant soliton spacing. Using Eq. (S5) and Eq. (S12a), this balance can be expressed as:

$$-\frac{2C_a\omega_s P_{\text{av}} L_{\text{PCF}}}{c} \frac{\delta_\Omega}{4\delta_\Omega^2 + \Gamma_B^2} \sin(\Omega_a \Delta t) = A_d B(\Delta\omega) \exp(-h\Delta t) \psi(\Delta\phi_0). \quad (\text{S13})$$

While the right side of the equation has a positive sign corresponding to a force of repulsion, a negative detuning of the lattice frequency from the mechanical resonance frequency ($\delta_\Omega < 0$) ensures that the optomechanical effect in the PCF creates an effective force of attraction between the two solitons. The theoretical fitting curves in Fig. 3B and Fig. 3D in main text are based on Eq. (S13).

When the system parameters are fixed, it can be seen that the intensity of the force of attraction on the left side of Eq. (S13) increases as the soliton spacing (Δt) increases, while the intensity of the force of repulsion on the right side of Eq. (S13) decreases as the soliton spacing increases. Such line shapes (see Fig. S4) are necessary to form a temporal trapping potential for the 2nd soliton (see Fig. 1E in the main text), which makes the long-range soliton binding robust.

S3. Soliton spacing tuning: Detailed discussion and supplementary experiments

S3.1. A schematic summary of the tuning process

The soliton spacing tuning of the ADS supramolecule was achieved by tailoring both the intensity of dispersive wave and the amplitude of mechanical vibration in the PCF core (see Fig. 3 in the main text). The principle of the soliton-spacing tuning process is schematically illustrated in Fig. S4, where the position of the 1st soliton in the double-soliton unit is set as the reference, and forces of attraction and repulsion are plotted in different colors with the line shapes that are described in S2 above. The crossing points of the two lines indicate the balanced positions for the 2nd soliton. As shown in Fig. S4A, a decrease in dispersive wave intensity would lead to a drop of the force of repulsion, resulting in a decrease in the soliton spacing. In practice, as the soliton spacing decreases, the force of attraction was also slightly varied since a shorter soliton spacing could lead simultaneously to slightly stronger mechanical vibrations in the PCF as shown in Eq. (S1). This effect, however, is neglected in Fig. S4A for simplicity. Similarly, as we gradually decrease the force of attraction with an almost invariant force of

repulsion, the balance between the two forces would lead to an increase in the soliton spacing (see Fig. S4B).

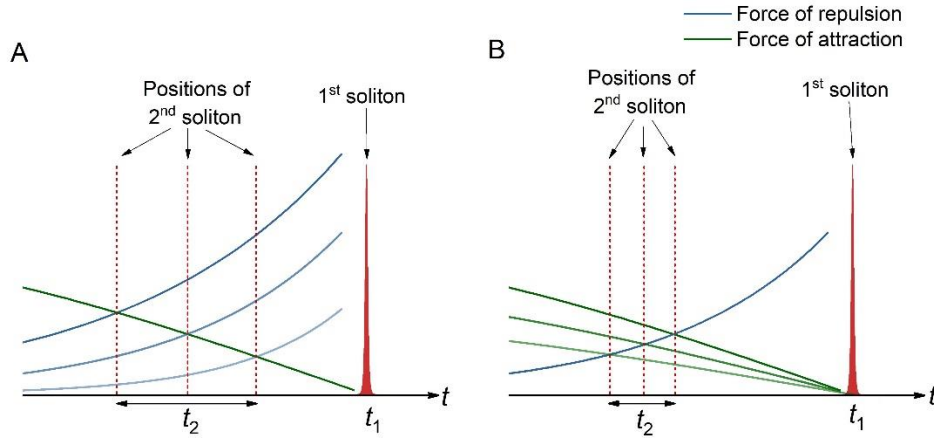


Fig. S4. Schematic illustration of the soliton spacing tuning in a double-soliton unit. (A) Tailoring of the dispersive wave leads to variations of the force of repulsion, and eventually results in shifts of the balanced position for the 2nd soliton. (B) Similarly, tailoring of the mechanical wave amplitude leads to variations of the force of attraction and therefore changes of the soliton spacing.

S3.2. Tailoring the forces of repulsion and attraction

In the experiments we varied the intensity of the $m=-1$ order dispersive wave by adjusting the cavity loss, which was implemented by adjusting the in-cavity tunable attenuator placed before the EDFA (see Fig. S1). When the total cavity loss was gradually varied from ~6 dB to ~11 dB, we observed that the intensity of the dominant Kelly sideband dropped by around three times (see Fig. 3A in the main text). In this process, the average optical energy out of the EDFA decreased, however, by less than 5%, which could be compensated by slightly increasing the pump power of the EDFA. The almost unchanged intra-cavity optical energy ensured that the optomechanical effect in the PCF was almost invariant. As illustrated in Fig. S4A, the decrease in the dispersive wave would result in a decrease of the force of repulsion between the two solitons, leading to a larger soliton spacing. In practice, while the basic structure of the ADS supramolecule was stably preserved in the laser cavity, the soliton spacing in the double-soliton unit could be tuned at will within a broad range from 40 ps to 116 ps. The maximum soliton spacing that we observed in the experiments was ~170 ps, achieved through increasing further the dispersive wave intensity. However, we need to use a higher pump power of the EDFA, leading to laser solitons with higher energies and broader spectra.

The soliton spacing could also be tuned through varying the force of attraction as illustrated in Fig. S4B. This was implemented by slightly adjusting the cavity length using the intra-cavity delay line (see Fig. S1). By gradually decreasing the cavity length, the free spectral range (FSR) of the cavity increased, corresponding to a tuning of the lattice frequency of the ADS supramolecule toward the mechanical resonance frequency of the PCF (see Fig. 3C). As the lattice frequency was tuned from 1.8725 GHz to 1.882 GHz, the soliton spacing in the double-soliton unit decreased from 87 ps to 63 ps (see Fig. 3D), which was induced by an increase of the force of attraction as illustrated in Fig. S4B. This tendency rolled over when we further increased the lattice frequency (see Fig. 3D), agreeing well with the theoretical predictions using Eq. (S13).

In experiments we could adjust the soliton spacing back and forth without destroying the ADS supramolecule. This continuous tunability could be attributed to the formation of

contactless binding of solitons within each time-slot of the optomechanical lattice (see section S2.3 above), highlighting the structural flexibility and reversibility of the supramolecular assembly of optical solitons.

S3.3. Supplementary results of soliton spacing tuning

By increasing the pump power of the EDFA, we could obtain an all-triple-soliton (ATS) supramolecule composed of triple-soliton units within all the time-slots of the lattice. The soliton spacing in the triple-soliton unit could also be tuned. In the experiments we observed that as we gradually varied the intensity of the $m=-1$ order dispersive wave (see Fig. S5A), the whole duration of the triple-soliton unit (Δt_{13} in Fig. S5B) could be tuned within a range of 102 ps to 187 ps and the spacing between the 1st and the 2nd soliton (Δt_{12} in Fig. S5B) could be tuned within a range of 50 ps to 95 ps.

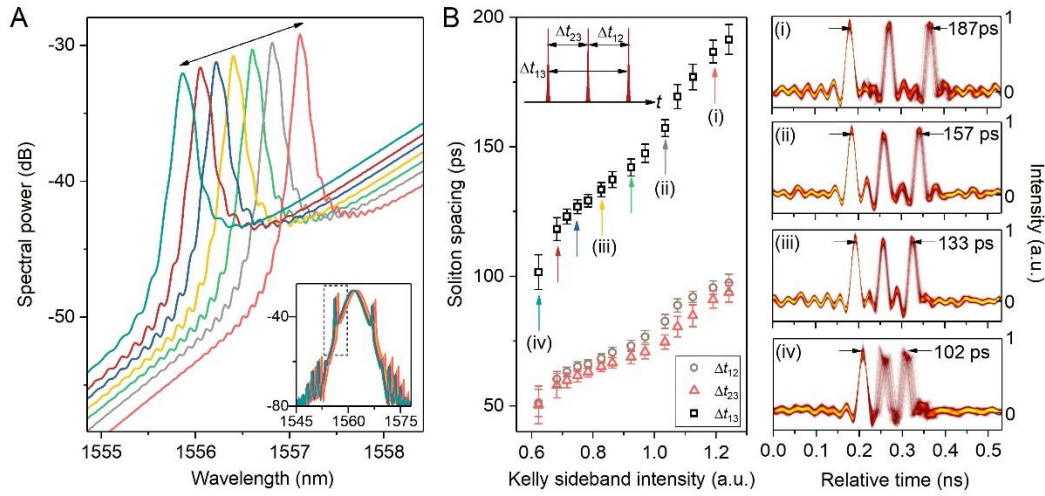


Fig. S5. Soliton spacing tuning of the all-triple-soliton supramolecule. (A) Tailoring of the intensity of the $m=-1$ order dispersive wave without changing spectral widths of the solitons (see the inset). (B) The soliton spacing increases as the dispersive wave grows. Δt_{12} , Δt_{23} and Δt_{13} are defined in the inset. Four examples are plotted in left columns (i) – (iv).

For measuring the soliton spacing, long-time averaging was used to obtain its mean value, and the root mean square of the spacing jitter was used for the error bars in Fig. 3B, Fig. 3D, and Fig. S5B. In the experiments, we observed slightly higher jitter spacing with an estimated maximum ~ 10 ps near the upper and lower edges of the tuning range, as shown in Fig. S5B for example. The large spacing jitters at the edges of tuning occur because we always optimized our system near the midpoint of the tuning range. Nevertheless, if all the system parameters were maintained in the recording, we did not observe degradation of the spacing jitter over time.

S4. Directions of Force of repulsion

The asymmetry of the laser spectrum could be induced by the asymmetric gain profile in the EDFA as well as the higher-order dispersion of the laser cavity (40). When we assume that the two Kelly-sidebands symmetrically located on the soliton spectrum (the absolute values of their deviations from the soliton central frequency are equal), asymmetric gain profile in the EDFA would impose different gain coefficients to the two first-order ($m=\pm 1$) Kelly-sidebands, leading to a difference between their stationary intensities. On the other hand, higher-order dispersion in the cavity would lead to an asymmetric distribution of the two sidebands on the soliton spectrum,

resulting in a difference in energy coupling from solitons (30, 39). In the experiments we could adjust the relative intensities of the two first-order sidebands by carefully adjusting the gain value in the EDFA (41) and the high-order dispersion in the cavity.

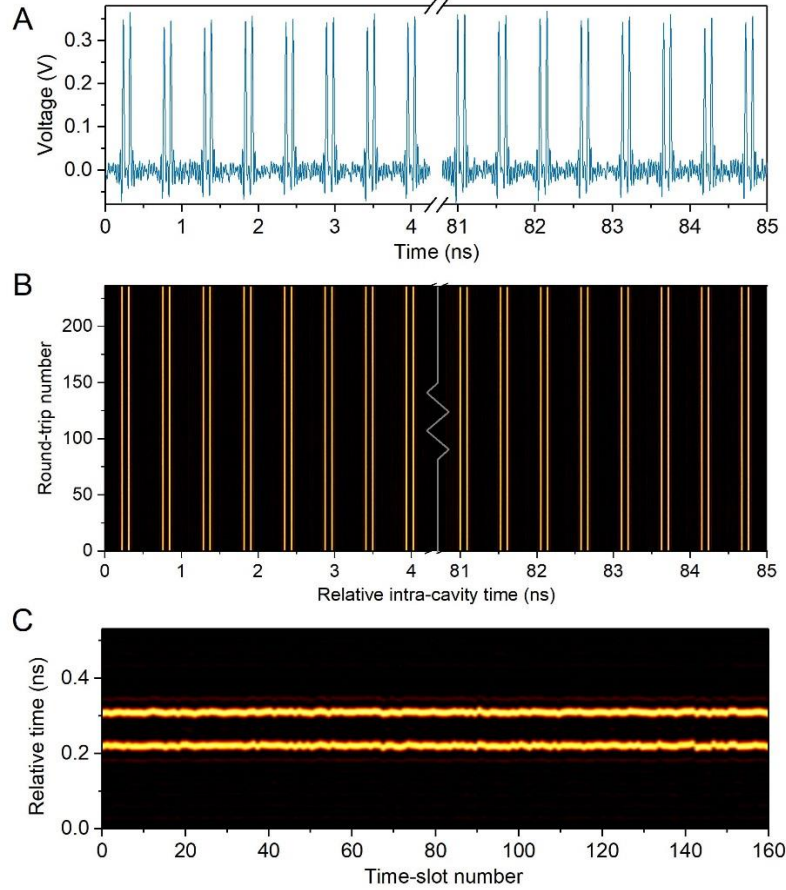


Fig. S6. Illustrations of the all-double-soliton supramolecule in three different ways. (A) Time-domain trace of the supramolecule recorded using the OSC. Due to the limit of figure size, the trace is plotted over only 8 ns (the cavity round-trip time was ~ 85 ns). (B) A plot of a longer time-domain trace over 230 cavity round-trips in the persistence mode. (C) The time-domain traces in the 160 time-slots of the lattice plotted in parallel. The vertical axis corresponds to the relative time in each time-slot (the period of lattice was ~ 0.531 ns), while the horizontal axis corresponds to the 160 consecutive time-slots.

Variations of relative intensities of the two sidebands could change the configuration of the force of repulsion due to dispersive wave perturbations, which has been verified in the experiments through plotting the soliton supramolecules in different ways. Figure S6A shows the ADS supramolecule recorded using the OSC over one cavity round-trip. As we increased the recording time, we could plot its time-domain trace over many cavity round-trips (the round-trip time was ~ 85 ns) in a persistence way as shown in Fig. S6B, which exhibits a perfect preservation of those double-soliton units in the optomechanical lattice. We also illustrate the experimental data in another way in which we separately plot the time-domain trace within each time-slot of the lattice (the period of the lattice was ~ 0.532 ns) along the ordinate in Fig. S6C, and we repeated such plot for the 160 consecutive time-slots along the abscissa in Fig. S6C, which exhibit the relative positions of the double-soliton units in the optomechanical lattice.

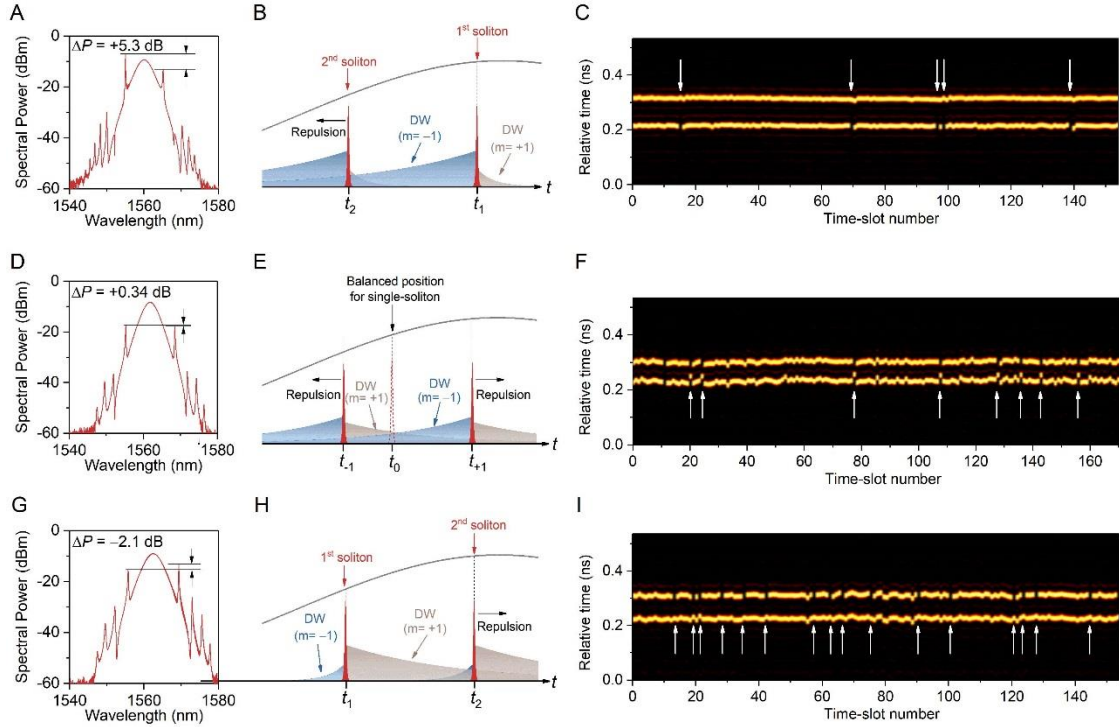


Fig. S7. Three cases of the force of repulsion due to dispersive wave perturbations. (A) The case that the $m=-1$ order sideband dominates. (B) The dispersive waves shed by the soliton are located later in time (set as the 1st soliton) perturbs the soliton located earlier in time, leading to an effective force of repulsion (C) The hybrid soliton supramolecule with several single-soliton units. The positions of those single-soliton units are marked by the white arrows (the upper row of pulses) (D) – (F) The two first-order ($m=\pm 1$) sidebands have comparable intensities in the second case. Both of these sidebands (dispersive waves) will contribute a force of repulsion between the two solitons, and push the two solitons in the double-soliton unit away from a balanced position. (G) – (I) When the $m=+1$ sideband dominates, the 1st soliton is earlier in time. The dispersive wave shed from this soliton travels slower than the soliton, and perturbs the 2nd soliton that is located later in time. We then find that the solitons in single-soliton units that are located at the same relative position as the 1st soliton in the double-soliton unit (the lower row of pulses in (I)).

By illustrating the hybrid soliton supramolecules, with one soliton or two contactlessly-bound solitons trapped in the time-slots of the lattice, in the same way as Fig. S6C, we can observe more information of the effective long-range force of repulsion between the two solitons due to dispersive wave perturbations. As shown in Fig. S7A, when the higher-frequency ($m=-1$ order) sideband dominates with an intensity difference $\Delta P=+5.3$ dB, we set the soliton located later in time as the reference (1st soliton) (see Fig. S7B). This is because that the force of repulsion in the double-soliton unit is merely induced by perturbation of the dispersive wave shed from the 1st soliton, and the $m=+1$ order dispersive wave shed from the 2nd soliton is much weaker. When a single soliton is trapped in one time-slot of the lattice, it is located in the same position as that of the 1st soliton in the double-soliton unit, since neither of them experiences significant perturbations from dispersive waves. As shown in Fig. S7C, in the experiments we recorded a hybrid soliton supramolecule including several time-slots with only one soliton trapped. In those single-soliton units (marked by white arrows in Fig. S7C), the solitons always locate at the “upper row” which corresponds to the later (the 1st soliton) position in Fig. S7B. In another case, as shown in Fig. S7D, comparable intensities of the two ($m=\pm 1$ order) sidebands ($\Delta P=+0.34$ dB) lead to two comparable perturbations of dispersive waves on both of the two

solitons (Fig. S7E), which push both of the two solitons away from the balanced position as shown in Fig. S7E and Fig. S7F. The last case is that the lower-frequency ($m=+1$ order) sideband dominates the force of repulsion with $\Delta P=-2.1$ dB (see Fig. S7G). In contrast to the first case shown in Fig. S7A–C, we use the soliton located earlier in time as the reference (1st) soliton in this case. The $m=+1$ order dispersive wave shed from the 1st soliton travels slower and perturbs the 2nd soliton located later in time (Fig. S7H). As a consequence, in single-soliton units the solitons always locate in the lower row (see Fig. S7I) which corresponds to the earlier soliton position in Fig. S7H.

We emphasize that in most of our experiments the $m=-1$ order sideband had the highest intensity and dominated the force of repulsion as shown in Fig. S7A and Fig. 3A in the main text. In the experiments, we did achieve almost uniform two ($m=\pm 1$ order) sidebands as shown in Fig. S7D and stronger $m=+1$ order sideband as shown in Fig. S7G through significantly increasing the cavity loss and simultaneously varying the cavity higher-order dispersion by changing the intra-cavity PCF length. The experimental results shown in Fig. S7 did not, however, alter the physical picture of the soliton supramolecules: two long-range soliton interactions work together to enable a large number of optical soliton to aggregate into supramolecular structures. Moreover, the results shown in Fig. S7 exhibit the universality of this supramolecular assembly of optical solitons which could be formed within a broad range of system parameters.

S5. Hybrid soliton supramolecules: Discussion and more examples

In the experiments we obtained a variety of hybrid soliton supramolecules composed of soliton units with different solitons numbers, which also showed perfect dynamic stability. This is attributed to the fact that the mechanical core resonance in the PCF has a lifetime of ~ 80 ns (30) which is comparable to the cavity round-trip time. The mechanical vibration in the PCF core driven by the supramolecules could not, therefore, respond to different soliton numbers in the time-slots of the optomechanical lattice. The excited mechanical vibration in the PCF core always has a sinusoidal waveform with an almost invariant amplitude which mainly depends on the laser average power in the PCF as shown in Eq. (S1).

The formation process of these hybrid soliton supramolecules depends critically on adjustments of PCs in the cavity. In this experiment, we could only partially control fine structures of the hybrid supramolecules. For example, we were able to reproducibly generate uniform structures with single-, double- or triple-soliton units in all the time-slots of the lattice. By varying the pump power in the EDFA, we could roughly control the total number of solitons in the supramolecular assembly. Independent control of the soliton number in each time-slot of the lattice has not been achieved at present. It should be possible however by further perfecting the previously-developed technique (21) to achieve this control. By launching a sequence of addressing pulses into the laser cavity, interactions between those addressing pulse sequence and intra-cavity soliton supramolecules might be used to generate encoded soliton supramolecules.

Besides the hybrid soliton supramolecule shown in Fig. 4C of the main text, two more examples are shown in Fig. S8. With a modest pump power in the EDFA, one hybrid soliton supramolecule with null-, single-, double-, and triple-soliton units could be obtained. In the experiments this hybrid supramolecule was also recorded at 5 min intervals over 20 min. The results are plotted in Fig. S8A, showing a long-term preservation of this supramolecular assembly in the freely-running fiber laser cavity. By increasing pump power in the EDFA, another hybrid soliton supramolecule with triple- and quadruple-soliton units filling in all the

time-slots of the optomechanical lattice was generated, and the results over a long-term recording are shown in Fig. S8B.

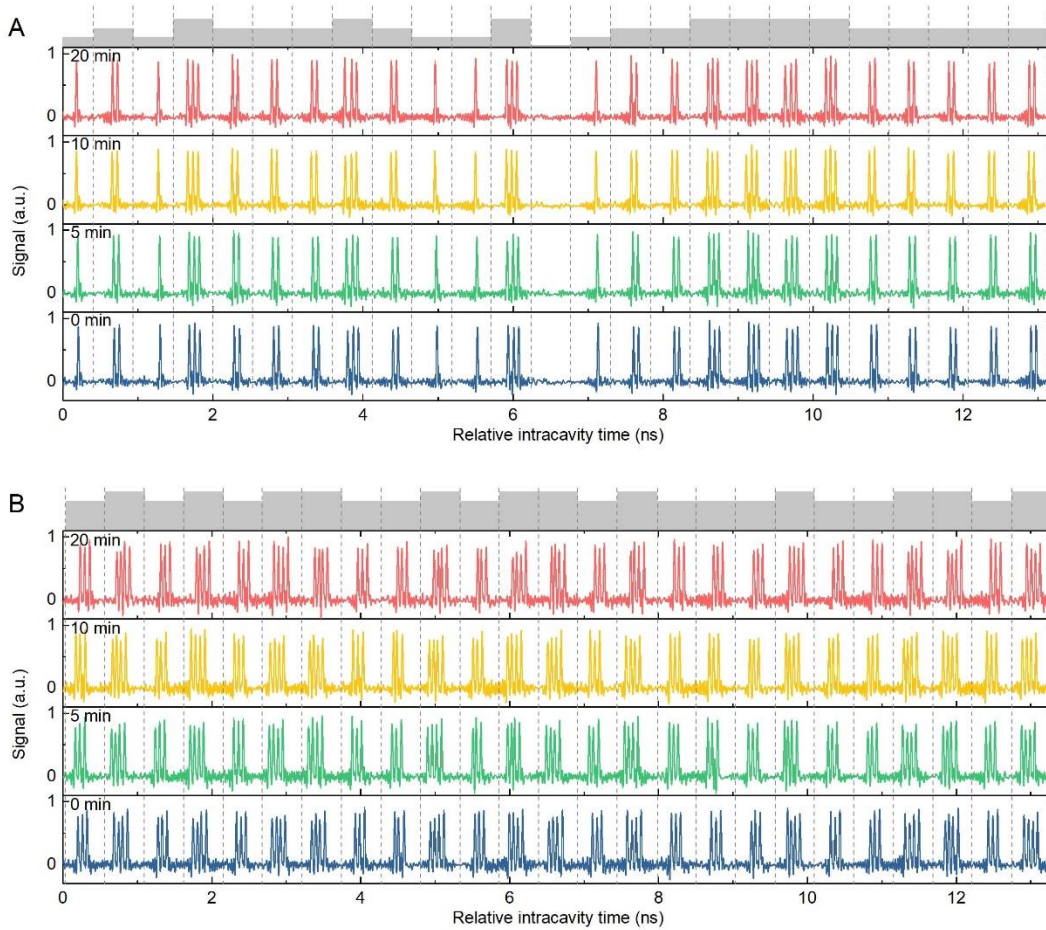


Fig. S8. Two examples of hybrid soliton supramolecules with long-term stability. (A) A hybrid soliton supramolecule composed of null-, single-, double-, and triple-soliton units in the time-slots of the lattice, obtained at a modest pump power in the EDFA. (B) Another hybrid soliton supramolecule composed of triple- and quadruple-soliton units, obtained at a higher EDFA pump power. Both of the two soliton supramolecules were recorded at 5 min intervals over 20 min. Data in only 25 consecutive time-slots are plotted due to the limited space.

A full record of the supramolecule that is partially plotted in Fig.S8A is shown in Fig. S9 below, containing the entire 160 time-slots within one cavity round-trip. Careful examination of the soliton number in each time-slot of this supramolecular assembly every 5 mins revealed that this highly-ordered structure was precisely preserved over the 20-min recording.

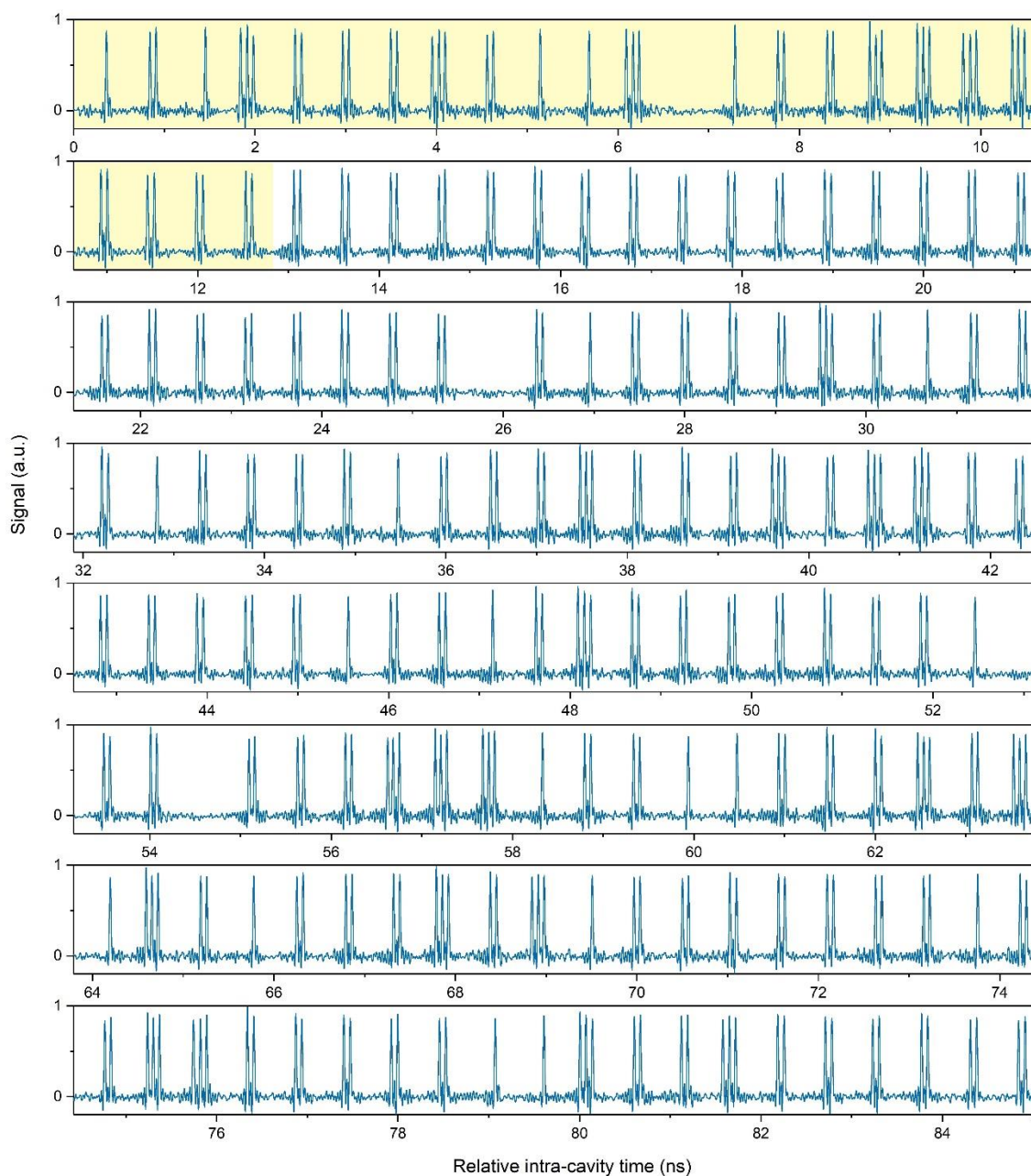


Fig. S9. Full record of the soliton supramolecule that is partially plotted in Fig.S8A, containing all the 160 time-slots. The results in the first 25 time-slots are highlighted in yellow.

Movie S1

Continuous tuning of the inner soliton spacing in the all-double-soliton supramolecule, achieved through tailoring the intensity of the $m=-1$ order dispersive wave.